DOI: 10.1002/ejic.200800572

Combined Experimental and Density Functional Theory Studies on the Crystal Structures and Magnetic Properties of $Mg(Mg_{1-x}Mn_x)_2Sb_2$ ($x \approx 0.25$) and $BaMn_2Sb_2$

Sheng-Qing Xia,[a] Chad Myers,[a] and Svilen Bobev*[a]

Keywords: Alloys / Density functional calculations / Manganese / Pnictides / Solid-state structures

Reported are the synthesis and structural characterization of two ternary transition metal intermetallic compounds, $Mg(Mg_{1-x}Mn_x)_2Sb_2$ (where x is approximately 0.25) and $BaMn_2Sb_2$·$Mg(Mg_{2.50(3)}Mn_{0.5})_2Sb_2$ crystallizes in the trigonal space group $P\bar{3}m1$ (no. 164) and belongs to the $CaAl_2Si_2$-type, while $BaMn_2Sb_2$ is isostructural with the body-centred tetragonal $ThCr_2Si_2$-type ($I4/mmm$, no. 139). Both structures have been refined from single-crystal X-ray diffraction data and their magnetic properties determined with the aid of a SQUID-magnetometry. The experimental results have been corroborated by electronic-structure calculations using the linear muffin-tin orbital (LMTO) method. Spin-polarized density-functional theory calculations confirm the antiferromagntically ordered magnetic structures.

Introduction

Intermetallic phases with the general formula AM_2X_2 (A = alkaline-earth or rare-earth metals, M = d-block metals; X = Group 13, 14 or 15 elements) comprise two ubiquitous structure types, $CaAl_2Si_2$ (Pearson's symbol $hP5$) and $ThCr_2Si_2$ (Pearson's symbol $tI10$), respectively.[1] There are close to a thousand known compounds with these two structures and their variants, and the chemical bonding in these systems has already been studied in great detail.[2–6] Over the past 2–3 decades, there has been a renewed interest in these materials due to a large number of attractive properties they possess: heavy fermions, superconductivity, mixed (or fluctional) valency, etc.[7–15] Of specific mention as well are the very recent reports identifying several AM_2Sb_2 antimonides as prospective materials for thermoelectric energy conversion.[16–19]

Our attention in these compounds, particularly in the AMn_2X_2 pnictides (A = Ca, Sr, Ba, Eu and Yb) was drawn after the realization that their peculiar magnetic behaviour arises from complex magnetic interactions within very simple atomic arrangements, e.g. $[Mn_2X_2]^{2-}$ layers of fused MnX_4 tetrahedra with A^{2+} cations packed between them. Take for example the phosphides $SrMn_2P_2$ ($CaAl_2Si_2$-type) and $BaMn_2P_2$ ($ThCr_2Si_2$-type), which remain antiferromagnetically ordered up to very high temperatures.[20] These experimental findings are also supported by spin-polarized density-functional theory calculations on the antimonides $CaMn_2Sb_2$ and $SrMn_2Sb_2$,[21] which suggest that the Mn atoms form two magnetic sub-lattices with strong ferromagnetic coupling within them and antiferromagnetic coupling between them.[21] Such magnetic ordering results in a negligible net effective magnetic moment, even though each Mn-ion in the structure is formally a high-spin Mn^{2+} and has five unpaired electrons.

Given that, one could expect that packing of the $[Mn_2Sb_2]^{2-}$ slabs with smaller or larger alkaline-earth cations, such as Mg^{2+} or Ba^{2+}, respectively, could disrupt the spin-coupling and change the ground state. A survey of the literature showed that $MgMn_2Sb_2$ is not known yet,[1] although α-Mg_3Sb_2 with the $CaAl_2Si_2$-type and its Zn-substituted variant $Mg(Mg_{1-x}Zn_x)_2Sb_2$ ($x < 0.7$)[19,22] are recognized to exist. This could be due to the fact that the melting point of the Mn is higher than the boiling point of Mg,[23] rendering the traditional high-temperature approach ineffective. We anticipated that using alternative routes, such as the metal-flux method,[24] this elusive compound can be readily synthesized.

On the other hand, $BaMn_2Sb_2$ was reported in 1979 to crystallize with the $ThCr_2Si_2$-type, and although its structure had been refined from singe-crystal work,[25] the published metric data, particularly the very high residuals (viz. $R_1 = 0.135$), leave this account somewhat doubtful. Surprisingly, almost 30 years later, there are still no reports on its properties, which prompted us to take a closer look at the Ba–Mn–Sb system and to re-access the synthesis and structure of this compound. We therefore embarked on combined experimental-computational studies of $MgMn_2Sb_2$

[a] Department of Chemistry and Biochemistry, University of Delaware,
Newark, DE 19716, USA
Fax: +1-302-831-6335
E-mail: bobev@udel.edu
Supporting information for this article is available on the WWW under http://www.eurjic.org or from the author.

and $BaMn_2Sb_2$, aimed at pinning down the structural parameters that affect most strongly the magnetism in these systems. Herein, we report the crystal and electronic band structures of $Mg(Mg_{1-x}Mn_x)_2Sb_2$ ($x \approx 0.25$) and $BaMn_2Sb_2$, in conjunction with their bulk magnetic properties.

Results and Discussion

Structure Description

The structure and the bonding in the $CaAl_2Si_2$ and $ThCr_2Si_2$ types have been given a full consideration in several earlier publications.[2–6] Therefore, only a brief description will be provided herein. The discussion will be focused on a few specific details of the structures, such as the stoichiometry breadth in $Mg(Mg_{1-x}Mn_x)_2Sb_2$ and its effect on the properties. Refined atomic parameters and interatomic distances are tabulated in Tables 1 and 2, respectively.

Table 1. Atomic coordinates and equivalent isotropic displacement parameters (U_{eq}) for $Mg(Mg_{1-x}Mn_x)_2Sb_2$ ($x \approx 0.25$) and $BaMn_2Sb_2$.

Atom	Site	x	y	z	U_{eq}[a] [Å^2]
		$Mg_{2.50(3)}Mn_{0.50(3)}Sb_2$			
Mg	1*a*	0	0	0	0.015(1)
M[b]	2*d*	1/3	2/3	0.6288(5)	0.016(1)
Sb	2*d*	1/3	2/3	0.2288(1)	0.014(1)
		$BaMn_2Sb_2$			
Ba	2*a*	0	0	0	0.015(1)
Mn	4*d*	0	1/2	1/4	0.015(1)
Sb	4*e*	0	0	0.3663(1)	0.014(1)

[a] U_{eq} is defined as 1/3 of the trace of the orthogonalized U_{ij} tensor. [b] M is refined as statistically occupied Mg and Mn in a ratio 0.751(16):0.249(16).

Table 2. Important bond lengths [Å] for $Mg(Mg_{1-x}Mn_x)_2Sb_2$ ($x \approx 0.25$) and $BaMn_2Sb_2$.

$Mg_{2.50(3)}Mn_{0.50(3)}Sb_2$			$BaMn_2Sb_2$		
Atom pair		Distance	Atom pair		Distance
Mg –	Sb × 6	3.086(2)	Ba –	Sb × 8	3.667(2)
M –	Sb × 3	2.804(2)	Mn –	Sb × 4	2.770(1)
	Sb	2.877(4)			
M –	M × 3	3.202(4)	Mn –	Mn × 4	3.120(1)

The structures of $Mg(Mg_{1-x}Mn_x)_2Sb_2$ and $BaMn_2Sb_2$ are schematically presented in Figure 1. Polyhedral representations are chosen to emphasize the $MnSb_4$ tetrahedra and the way they are connected. The former structure is with the trigonal space group $P\bar{3}m1$ (No. 164) and belongs to the $CaAl_2Si_2$-type.[1] There are three crystallographically unique sites in the asymmetric unit and one of them is occupied by statistical mixture of Mn and Mg (see Experimental). This atomic arrangement can be related to that of α-Mg_3Sb_2,[19] where every 4th Mg occupying the tetrahedral site (2d) is randomly substituted by Mn. Full replacement of Mg by Mn at this site would result in double corrugated $[Mn_2Sb_2]^{2-}$ layers, identical to those in $CaMn_2Sb_2$ and $SrMn_2Sb_2$.[21] These 2D-layers are built through corner- and edge-shared tetrahedra as shown in Figure 1. Such polyanionic network can be derived by puckering of "dimerized" honeycomb layers or by splitting of wurtzite-type 3D-lattice, followed by a subsequent reconstruction.[2] Divalent cations, Mg^{2+}, Ca^{2+}, Sr^{2+} fill the octahedral cavities between neighbouring layers.

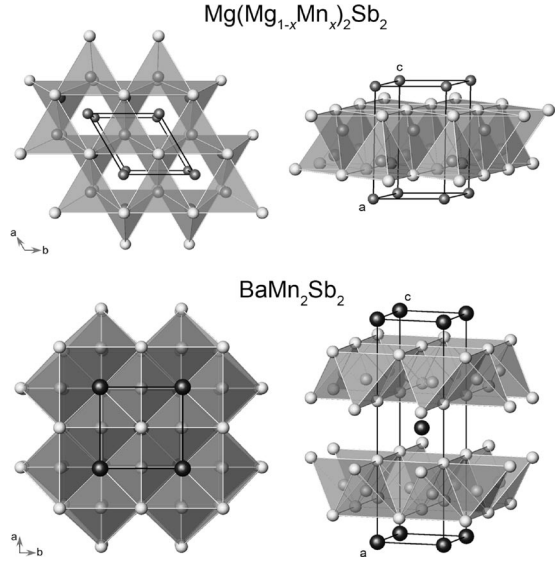

Figure 1. Polyhedral representations of the structures of $Mg(Mg_{1-x}Mn_x)_2Sb_2$ (top) and $BaMn_2Sb_2$ (bottom), shown in two different orientations. Unit cells and viewing directions are depicted. Sb atoms are shown as light grey spheres, Mg and Ba atoms are drawn in dark grey and black, respectively. The mixed Mn–Mg sites in $Mg(Mg_{1-x}Mn_x)_2Sb_2$ and the Mn atoms in the $BaMn_2Sb_2$ structure are shown as the centres of translucent tetrahedra.

$BaMn_2Sb_2$ crystallizes with the $ThCr_2Si_2$-type[1] in the body-centred tetragonal space group *I*4/*mmm* (No. 139). There are again three crystallographically unique sites in the asymmetric unit, which are occupied by Ba (2*a*), Mn (4*d*) and Sb (4*e*), respectively. There is no disorder in this structure, confirming the previous report.[25] The structure can be viewed as $Mn_2Sb_2^{2-}$ layers, which are built of $MnSb_4$ tetrahedra that share edges in a PbO-like pattern (Figure 1). The layers are stacked along the direction of the *c*-axis leaving large "cubic" holes between them. They are filled with the Ba^{2+} cations. This difference between the six- vs. eight-coordinate geometry of the cations sandwiched between the $[Mn_2Sb_2]^{2-}$ layers here in the above-discussed $Mg(Mg_{1-x}Mn_x)_2Sb_2$ may explain why $BaMn_2Sb_2$ forms with the $ThCr_2Si_2$ structure, while the Mg, Ca and Sr analogs form with the $CaAl_2Si_2$ structure – the increasing of the coordination number from Mg^{2+} to Ba^{2+} can be explained by the Pauling's rules,[26] which relate the coordination environment of the cations to the ratio of the radii of the corresponding cations and anions.

Another prominent feature that deserves further attention is the Mg–Mn disorder in $Mg(Mg_{1-x}Mn_x)_2Sb_2$. As mentioned above, this is not the first instance of a mixing between a d-metal and Mg within this structure. Indeed, our earlier work with Mg and Sb in excess of Zn, intended as a self-flux, yielded large crystals of the compound

$Mg(Mg_{1-x}Zn_x)_2Sb_2$ ($x \approx 0.7$).[22] It is isostructural to the herein discussed Mn-analog and also exhibits substantial mixing of Zn and Mg on the very same crystallographic site. These findings are complemented by the work of Ahmadpour et al.,[19c] which estimates the phase width to vary between 0 and 70 at.-% Zn, depending on the synthetic conditions. In a direct comparison, the homogeneity range for $Mg(Mg_{1-x}Mn_x)_2Sb_2$ ($x \approx 0.25$) appears to be much narrower. According to the results summarized in Table 3, the maximum amount of Mn in the structure is on the order of 25 at.-%. A comparison of the Pauling's metallic radii of Mg, Zn and Mn, which are 1.364, 1.213 and 1.178 Å,[26] respectively, provides clues as to how to account for these results. Evidently, the closer the radii, the easier the substitution would be, provided that the valence electron concentration does not change (Mn and Zn are d^5 and d^{10} metals and contribute to the bonding the same number of valence electrons as Mg). Hence, the less-favourable substitution rate for Mn can be correlated to the greater mismatch between the Mg and Mn radii compared to Mg and Zn. Another way to reconcile these findings requires us to recall the detailed theoretical analysis on this structure by R. Hoffmann and co-workers.[2] According to it, the Sb–M contacts parallel to the direction of the *c*-axis (aka "handle" bonds) will be systematically shorter than the Sb–M contacts in the *ab*-plane (aka "rib" bonds) only when the transition metal has half-filled d-bands.[2] This is not the case with $Mg(Mg_{1-x}Mn_x)_2Sb_2$ as the "handle" bonds are almost 0.08 Å longer than the "rib" bonds (Table 2). This subtlety of the bonding within the layers provides for almost no interference for the replacement of Mg atoms with Zn ($3d^{10}$), but hinders the incorporation of the Mn atoms ($3d^5$) into the layers – an excellent agreement between theory and our experimental results in that regard.

Table 3. Unit cell parameters for different samples of $Mg(Mg_{1-x}Mn_x)_2Sb_2$. The data were refined by least-square fits of the positions of the peaks from the powder X-ray diffraction patterns (room temperature), using Si as an internal standard.

No.	Nominal composition Mg/Mn/Sb	Unit cell parameters
I	1:2:2	a = 4.539(3); c = 7.226(3) V = 128.93 Å^3
II	2.5:0.5:2	a = 4.550(4); c = 7.228(4) V = 129.59 Å^3
III	2.75:0.25:2	a = 4.552(3); c = 7.227(3) V = 129.70 Å^3
	Mg_3Sb_2	a = 4.55876(7); c = 7.2274(2)[a] V = 130.08 Å^3

[a] Taken from ref.[19c].

The relatively poor "solubility" of Mn and the corresponding narrow stoichiometry breadth in $Mg(Mg_{1-x}Mn_x)_2Sb_2$ have an important synthetic implication, which is also clearly seen from Table 3 – a large excess of Mn is needed in order to achieve higher substitution rate. For example, sample I with nominal composition of Mg/Mn/Sb = 1:2:2 yields a product that has significantly lesser amount of Mn.[27] Although no structure refinements were carried out for these polycrystalline samples, from the gradual increase of the unit cell volume and the closeness of the metric parameters to those of α-Mg_3Sb_2,[19] it is evident that the percent Mn that substitutes for Mg is very low. As a result of this synthetic limitation, polycrystalline samples prepared by direct fusion of the elements are inherently contaminated with left-over Mn or unwanted MnSb. The presence of secondary phase(s) hampers the magnetic and transport property measurements on such samples and requires the use of the flux-method for the synthesis of single-crystalline specimens.

Magnetic Susceptibility

The temperature dependence of the magnetic susceptibility data of $Mg(Mg_{1-x}Mn_x)_2Sb_2$ ($x \approx 0.25$) is plotted in Figure 2. The compound show paramagnetic behaviour in the measured temperature range (5–290 K), which is in sharp contrast with the results from the isostructural compounds $CaMn_2Sb_2$ or $SrMn_2Sb_2$.[21] Unlike $CaMn_2Sb_2$ or $SrMn_2Sb_2$, the magnetization of $Mg(Mg_{1-x}Mn_x)_2Sb_2$ ($x \approx 0.25$) shows obvious temperature dependence, reminiscent with Curie-like paramagnetic behaviour. However, the dependence of the inverse susceptibility with the temperature is not linear, precluding a fit of the $\chi^{-1}(T)$ data to the Curie law.[28] Therefore, to estimate the effective moment, a nonlinear fit of the data based on the Curie–Weiss equation $\chi(T) = \chi_o + C/(T - \theta_p)$ was applied. Here, χ_o is the sum of the temperature-independent contributions, e.g. van Vleck paramagnetism, paramagnetism due to conduction electrons and core-electron diamagnetism ($C = N_A\mu_{eff}^2/3k_B$ is the Curie constant, where N_A is the Avogadro number and k_B is the Boltzmann constant) and θ_p is the Weiss constant.[28] This fitting procedure yielded an effective moment of μ_{eff} = 1.8 μ_B per Mn, significantly lower than the theoretically predicted spin-only effective moment μ_{eff} = 5.9 μ_B for a free Mn^{2+} ion with 5 unpaired electrons.[28] This low moment is most likely suggestive of a complex magnetic structure and cannot be taken as an indication of either a low-spin state or highly oxidized Mn^{n+} configuration ($n > 2$). Discussion of the possible magnetic structure follows; as elaborated therein and as argued elsewhere,[29–33] Mn^{3+} or higher oxidation states for Mn are not expected to be stable in antimonides and pnictides in general.

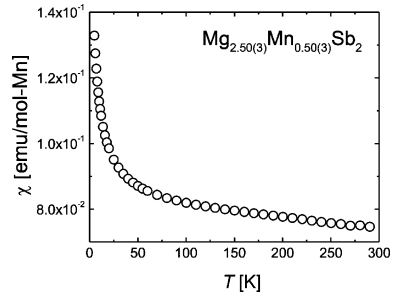

Figure 2. Temperature dependence of the magnetic susceptibility of $Mg(Mg_{1-x}Mn_x)_2Sb_2$ ($x \approx 0.25$), cooled from room temperature to 5 K at an applied field H = 5000 Oe.

The magnetic behaviour of $BaMn_2Sb_2$ appears very similar to that of the isostructural $BaMn_2P_2$.[20] The magnetic susceptibility (χ) of $BaMn_2Sb_2$ decreases slowly as the temperature is lowered from 290 to ca. 75 K, and then increases (Figure 3). For both compounds, no maxima in the magnetic susceptibility can be observed from 5 K up to room temperature. Such χ vs. T dependence could signify a strong antiferromagnetic order, which was confirmed for $BaMn_2P_2$ from both magnetic susceptibility measurements and variable temperature neutron diffraction experiments (Néel temperature $T_N \approx 750$ K).[20] However, the expected high ordering temperature for $BaMn_2Sb_2$ could not be experimentally verified due to its air-sensitivity and the specialized nature of such measurements. Nonetheless, the antiferromagnetic ground state for $BaMn_2Sb_2$ is evidenced from the spin-polarized calculations, discussed in detail next.

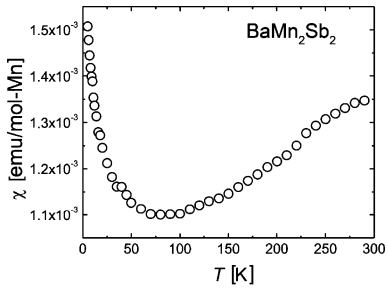

Figure 3. Temperature dependence of the magnetic susceptibility of $BaMn_2Sb_2$, cooled from room temperature to 5 K at an applied field 5000 Oe.

Electronic Structure

To understand the magnetic properties of $Mg(Mg_{1-x}Mn_x)_2Sb_2$ and $BaMn_2Sb_2$, electronic structure calculations were performed on these compounds based on the Tight-Binding LMTO method using the atomic-sphere approximation. The total DOS together with the partial DOS of the Mn 3d-orbital for the idealized $MgMn_2Sb_2$ structure are plotted in Figure 4. The corresponding DOS curves of

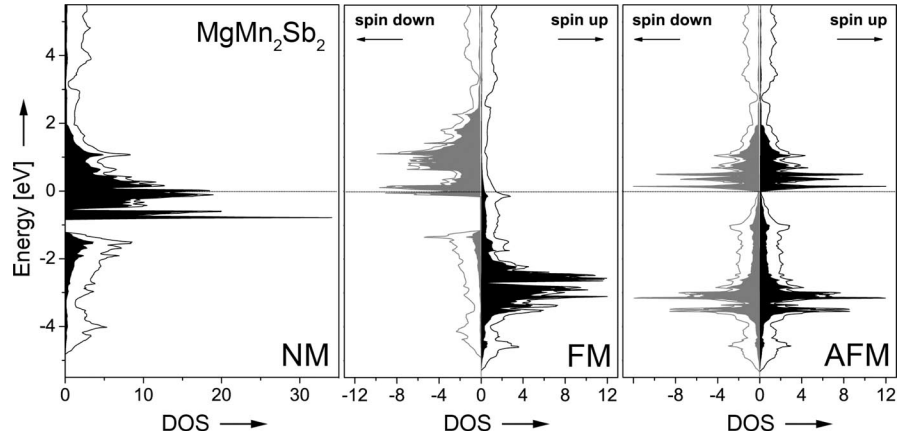

Figure 4. Density of states (DOS) for the idealized $MgMn_2Sb_2$ compound ($CaAl_2Si_2$-type). Total (solid line) and partial (shaded area) DOS of the 3d orbitals of Mn are shown. The calculations are performed assuming a nonmagnetic (*NM*) structure, or structures with ferromagnetically (*FM*) and antiferromagnetically (*AFM*) coupled Mn spins, respectively.

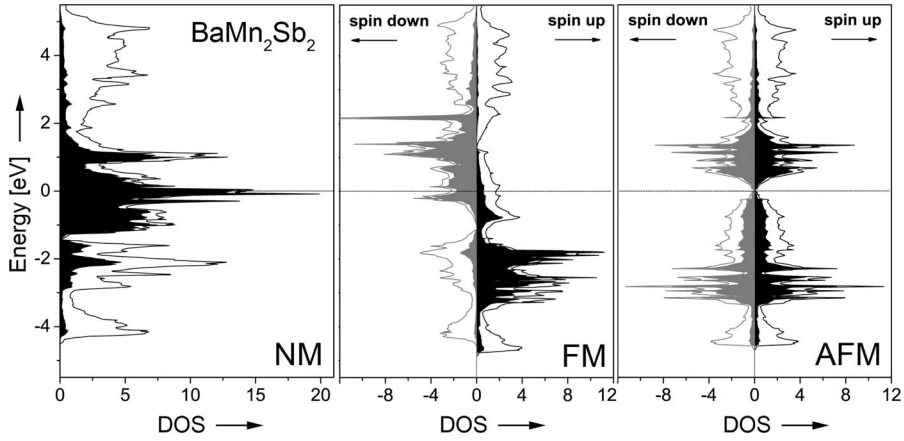

Figure 5. Density of states (DOS) for $BaMn_2Sb_2$ ($ThCr_2Si_2$-type). Total (solid line) and partial (shaded area) DOS of the 3d orbitals of Mn are shown. The calculations are performed for the nonmagnetic (*NM*) structure, or structures with ferromagnetically (*FM*) and antiferromagnetically (*AFM*) coupled Mn spins, respectively.

$BaMn_2Sb_2$ are plotted in Figure 5. Three different models, nonmagnetic (*NM*), ferromagnetic (*FM*) and antiferromagnetic (*AFM*) are calculated for both structures. According to the calculations, both $MgMn_2Sb_2$ and $BaMn_2Sb_2$ should be antiferromagnetic (*AFM*) in their ground state, since the calculations for the *AFM*-ordered structures suggest most optimized bonding picture. The respective *AFM* models for $MgMn_2Sb_2$ and $BaMn_2Sb_2$ are schematically represented in Figure 6. Closer inspections of the bands that are in a close vicinity of the Fermi level reveals that they are predominantly contributed by 3d orbitals of Mn, which indicates that they will be important for the electronic properties of these compounds. There is negligible DOS at the Fermi level, hence, the conductivity is expected to be poor.[34] Such conclusion is further corroborated by a four-probe electrical resistivity measurement on a single crystal of $Mg(Mg_{1-x}Mn_x)_2Sb_2$ (see ESI). This is also consistent with earlier reports on other AMn_2Sb_2 antimonides (A = Ca, Sr, Yb, Eu) with the same structures.[20,21,35,36]

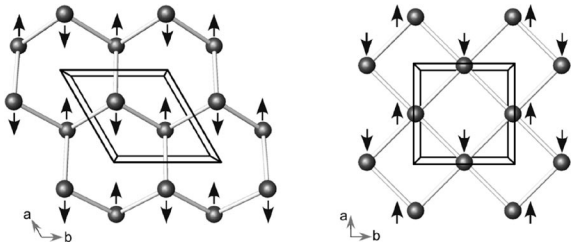

Figure 6. Schematic representations of the *AFM* models for the idealized $MgMn_2Sb_2$ structure (left) and the $BaMn_2Sb_2$ structure (right) from the TB-LMTO-ASA calculations. For clarity, only the Mn-substructures are shown and the corresponding unit cells are outlined.

Comparisons of the calculated local moment of Mn and the total energies for each of the selected models of $BaMn_2Sb_2$ are presented in Table 4. The same type of analysis for $MgMn_2Sb_2$ is provided as Supporting Information. From Table 4, it is evident that the total energies calculated for the *FM* and *AFM* models are always much lower than the *NM* one, with the *AFM* model giving the most stable configuration. These results are suggestive of a very strong Mn–Mn antiferromagnetic coupling in both $MgMn_2Sb_2$ and $BaMn_2Sb_2$. The local moment for each Mn atom is calculated to be almost 4 μ_B, which is in good agreement with the earlier neutron diffraction results for $SrMn_2P_2$ and $BaMn_2P_2$,[20] as well as the computations for $CaMn_2Sb_2$ and $SrMn_2Sb_2$.[21] According to these, Mn in this structure should be interpreted as high-spin Mn^{2+}.

Although the calculations provided a good overall picture of the electronic structure for both compounds, they cannot explain the apparent temperature dependence of the magnetic susceptibility observed for $Mg(Mg_{1-x}Mn_x)_2Sb_2$ (Figure 2). Therefore, additional calculations were performed for the latter using a model $2\times2\times1$ super-cell. The rational for creating the hypothetical $Mg_{10}Mn_2Sb_8$ compound (i.e., $4\times Mg_{2.50(3)}Mn_{0.50(3)}Sb_2$) originated from the observation that on the 2*d* site (Table 1), virtually every 4th Mg atom is replaced by Mn. Based on that, three likely

Table 4. Theoretically calculated (LDA or GGA) local magnetic moments (μ) for the Mn atoms and relative total electronic energies (E_{TOT}) for $BaMn_2Sb_2$. The energy difference ($\Delta E = E_{AFM} - E_{FM}$) between the *AFM* and *FM* models is also shown. The total energy of the corresponding *NM* ground states is selected as an energy reference.

Method	Ground state	μ_{Mn} [μ_B]	E_{TOT} [eV]	ΔE [meV/Mn]
LDA	*NM*	0	0	
	FM	3.56	–1.136	–232
	AFM	3.74	–1.599	
GGA	*NM*	0	0	
	FM	3.71	–1.522	–214
	AFM	3.87	–1.950	

ordered models were chosen for in-depth analyses, as they exemplify three very different Mn–Mn types of long-range order. These models are schematically illustrated in Figure 7. The total energies calculated for them are listed in Table 5. To compare their relative stabilities, the nonmagnetic total energy of model **I** was chosen as an energy reference. Based on the *NM* calculations, model **II** is suggested to be the most stable one, with a total energy that is lower by 0.903 eV (LDA) and 0.938 eV (GGA) compared to model **I**. Model **III** is the least stable one (Table 5).

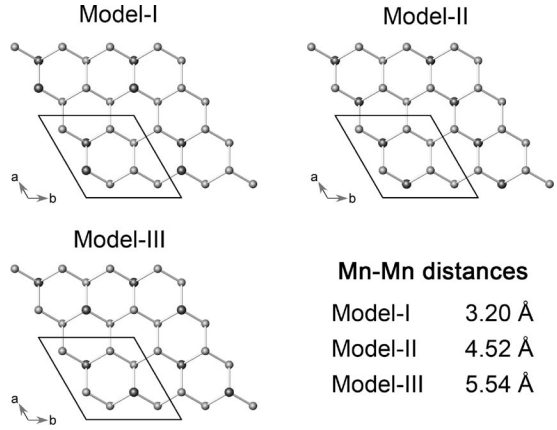

Figure 7. Schematic representation of three likely $Mg_{10}Mn_2Sb_8$ structures, formed in $2\times2\times1$ super-cells of $Mg(Mg_{1-x}Mn_x)_2Sb_2$ ($x \approx 0.25$). The corresponding Mn–Mn distances are indicated in the figure. Mn atoms are shown as darker spheres.

Table 5. Theoretically calculated (LDA or GGA) relative total electronic energies (E_{TOT}) for three hypothetical $Mg_{10}Mn_2Sb_8$ structures, built from $Mg(Mg_{1-x}Mn_x)_2Sb_2$ ($x \approx 0.25$) using $2\times2\times1$ super-cells. The energy difference ($\Delta E = E_{AFM} - E_{FM}$) between the *AFM* and *FM* models is also shown. The total energy of the corresponding *NM* ground state for model **I** (shortest Mn–Mn distance) is selected as an energy reference.

Ground state	Model **I**		Model **II**		Model **III**	
	LDA	GGA	LDA	GGA	LDA	GGA
NM	0	0	–0.903	–0.938	0.303	0.310
FM	–3.265	–3.771	–4.050	–4.605	–3.133	–3.628
AFM	–3.537	–4.024	–4.300	–4.842	–3.282	–3.764
ΔE [meV/Mn]	–136	–126	–125	–118	–74	–68

Spin-polarization calculations were also performed for these hypothetical structural models by treating two of the

Mn atoms in the unit cell to be ferromagnetically (*FM*) or antiferromagnetically (*AFM*) coupled. According the energy differences between the *FM* and *AFM* magnetic calculations, strong antiferromagnetic Mn–Mn interactions are expected for all three different structural models. Again, for model **II**, the *AFM* alignment gives the lowest total energy (both LDA and GGA) compared to the other two models. From the above, it is easy to explain why the observed effective moment is much lower than the expected 5.9 μ_B for high-spin Mn^{2+}. However, the observed temperature dependence of the magnetic susceptibility of $Mg(Mg_{1-x}Mn_x)_2Sb_2$ ($x \approx 0.25$) and the existence of a nonzero effective moment remain open questions. Several possible reasons may account for this: first, the actual composition might be slightly different from the idealized $Mg_{10}Mn_2Sb_8$ one (i.e., $Mg_{2.5}Mn_{0.5}Sb_2$), resulting in a small amount of "uncompensated spins"; second, the models discussed above are probably too simple to describe the real structure; and third, small paramagnetic impurity might be present. The latter is not as likely as the first two reasons since the magnetic properties were determined for selected single crystals and were found to be reproducible within different reaction batches. Therefore, we argue that the actual magnetic structure is more complicated, involving possibly short-range correlations, non-random or domain-like distributions of Mn, lattice dynamics, cluster spin-glass behaviour, etc. Such "non-localities" and deviations for the ordered, or for that matter fully disordered models that were discussed herein can, of course strongly influence the long-range properties.

Conclusions

Single-crystals of $Mg_{2.50(3)}Mn_{0.50(3)}Sb_2$ and $BaMn_2Sb_2$ have been grown using the metal-flux method. The crystal structures of the two compounds have been established by single-crystal X-ray diffraction. Their bulk magnetic properties have been studied by magnetization measurements in the temperature range from 5 to 290 K. The experimental results have been complimented by electronic structure calculations and spin-polarization calculations, using the TB-LMTO-ASA method. For the stoichiometric compound $BaMn_2Sb_2$, the experiment and the calculations confirm the existence of a strong antiferromagnetic order. Model calculations for the solid solution $Mg(Mg_{1-x}Mn_x)_2Sb_2$ ($x \approx 0.25$) also suggest very strong antiferromangetic coupling; however, the magnetic susceptibility of $Mg_{2.50(3)}Mn_{0.50(3)}Sb_2$ shows Curie-like paramagnetic behaviour, which is not consistent with the computations. We have argued that the actual magnetic order is perhaps more complicated, which calls for further neutron diffraction or X-ray magnetic circular dichroism (XMCD) studies. Because $Mg(Mg_{1-x}Mn_x)_2Sb_2$ is a substitution derivative of α-Mg_3Sb_2, which is nominally a Zintl phase and a small band-gap semiconductor, an appropriate and controlled replacement of Mg by Mn can result in dilute magnetic semiconductor with interesting physical properties.

Experimental Section

Synthesis: Single crystals of $Mg(Mg_{1-x}Mn_x)_2Sb_2$ and $BaMn_2Sb_2$ were grown from high-temperature reactions using Sn as metal flux.[24] The starting materials were purchased from Alfa or Aldrich and used as received (stated purity greater than 99.9%). The metals were stored and handled inside an argon-filled glove box or under vacuum in order to prevent unwanted oxidation. The synthetic procedure was identical to that used for the crystal growth of $CaMn_2Sb_2$ and $SrMn_2Sb_2$ and was described in detail elsewhere.[21] The products of the flux reactions in both cases were thin plates, later identified as the title compounds. In the Mg–Mn–Sb reactions, where Mn was used in excess, small needle crystals of MnSb[37] were obtained as a side product.

Although this study dealt exclusively with single crystals, we note here that $Mg(Mg_{1-x}Mn_x)_2Sb_2$ and $BaMn_2Sb_2$ can be synthesized in a polycrystalline form through stoichiometric reactions in welded Nb-ampoules. This was not the method of choice herein primarily because the Nb tubes become susceptible to side reactions at temperatures above 1000 °C, resulting in the contamination of the samples with Nb–Sb binaries. Another drawback of the direct fusion method with regard the synthesis of phase-pure $Mg(Mg_{1-x}Mn_x)_2Sb_2$ samples has been discussed (see Results and Discussion).

The crystals of $BaMn_2Sb_2$ appeared moderately sensitive to air, as evidenced from the quick loss of their luster when left in the open atmosphere. The crystals of $Mg(Mg_{1-x}Mn_x)_2Sb_2$ in turn were found to be stable in air for several weeks.

X-ray Powder Diffraction: All powder X-ray diffraction patterns were taken at room temperature on a Rigaku MiniFlex powder diffractometer using Cu-K_α radiation. The data analysis was carried out employing the JADE 6.5 software package. The patterns were used to analyze the products from the reactions and to investigate the possible phase width existing in $Mg(Mg_{1-x}Mn_x)_2Sb_2$. Specifically, powder patterns were taken for all samples prepared with various nominal compositions (Table 3). The unit cell parameters in each case were refined by the least-squares method and the patterns were calibrated with Si as an internal standard.

Single Crystal X-ray Diffraction: Single crystals of the title compounds were picked, cut to suitable sizes for data collection [$70 \times 30 \times 30$ μm^3 for $Mg(Mg_{1-x}Mn_x)_2Sb_2$ and $100 \times 40 \times 40$ μm^3 for $BaMn_2Sb_2$], and mounted on glass fibers using Paratone N oil. Intensity data collections were carried out at 120(2) K on a Bruker SMART CCD-based diffractometer. Nearly full spheres of reciprocal space data were collected in four batch runs at different ω and ϕ angles (up to $2\theta_{max} \approx 55°$). The data collections were handled using the SMART software,[38] data integrations and global unit cell refinements were done with the SAINTplus program.[38] Semi-empirical absorption correction based on equivalents was applied using SADABS[39] [T_{min}/T_{max} = 0.683 and R_{int} = 0.0505 for $Mg_{2.50(3)}Mn_{0.50(3)}Sb_2$, T_{min}/T_{max} = 0.471 and R_{int} = 0.0378 for $BaMn_2Sb_2$, respectively]. The structures were refined by full-matrix least-squares methods on F^2 using the SHELX package.[40] Refined parameters included the scaling factors, atomic positions and the anisotropic displacement parameters. Selected data collection and refinement parameters are given in Table 6 below; refined atomic parameters and relevant bond lengths are listed in Tables 1 and 2. Further information in the form of CIF has been deposited with Fachinformationszentrum Karlsruhe, 76344 Eggenstein-Leopoldshafen, Germany, [Fax: +49-7247-808-666; E-mail: crysdata@fiz.karlsruhe.de] – depository number CSD-419530 (for $Mg_{2.50(3)}Mn_{0.50(3)}Sb_2$), -419531 (for $BaMn_2Sb_2$), respectively.

Table 6. Selected crystallographic data for $Mg(Mg_{1-x}Mn_x)_2Sb_2$ ($x \approx 0.25$) and $BaMn_2Sb_2$.

Chemical formula	$Mg_{2.50(3)}Mn_{0.50(3)}Sb_2$	$BaMn_2Sb_2$
Formula weight	331.74	490.72
Space group, Z	$P\bar{3}m1$ (No. 164), 1	$I4/mmm$ (No. 139), 2
Unit cell parameters	a = 4.522(3) Å	a = 4.412(2) Å
	c = 7.191(5) Å	c = 14.414(8)
	V = 127.36(14) Å^3	V = 280.6(2) Å^3
Radiation, λ	Mo-K_α, 0.71073 Å	
T [K]	120(2)	
$\rho_{calcd.}$ [g/cm^3]	4.325	5.808
μ [mm^{-1}]	11.905	20.622
Goodness of fit on F^2	0.938	1.066
Final R_1 ($I > 2\sigma_I$)[a]	0.0239	0.0304
Final wR_2 ($I > 2\sigma_I$)[b]	0.0501	0.0695

[a] $R_1 = \Sigma||F_o| - |F_c||/\Sigma|F_o|$. [b] $wR_2 = [\Sigma[w(F_o^2 - F_c^2)^2]/\Sigma[w(F_o^2)^2]]^{1/2}$.

We also note trial refinements of the occupancies for the sites, done by freeing the site occupation factor (SOF) for an individual atom while the remaining SOF's were kept fixed. They proved that the corresponding deviations from full occupancy are within 3σ for all sites, except for the position labeled "M" in the $Mg(Mg_{1-x}Mn_x)_2Sb_2$ structure (Table 1). Its site occupation factor indicated scattering from a heavier than Mg but lighter than Mn atom and was therefore modeled by refining it as a statistical mixture of 25(2)% Mn and 75(2)% Mg, respectively.

Elemental Microanalysis: To independently verify that $Mg(Mg_{1-x}Mn_x)_2Sb_2$ is not a line compound, two different crystals that were synthesized from reactions with different ratios of the starting materials were subjected to elemental analysis by means of SEM-EDX. The crystals were mounted onto a carbon tape and placed in the chamber of a Jeol 7400 F electron microscope equipped with an INCA-Oxford energy-dispersive spectrometer. The microscope was operated at 10 μA beam current at 15 kV accelerating potential. Several measurements were taken for each and then averaged. The normalized per antimony compositions were $Mg_{2.3}Mn_{0.5}Sb_2$ and $Mg_{2.5}Mn_{0.3}Sb_2$, consistent with the above-discussed results.

Magnetic Susceptibility: Temperature-dependent magnetic-susceptibility data were acquired with a Quantum Design MPMS SQUID magnetometer. The samples consisted of carefully selected crystals of $Mg_{2.50(3)}Mn_{0.50(3)}Sb_2$ (15 mg) and $BaMn_2Sb_2$ (9 mg), which were subsequently placed in custom-designed capsules.[30] The measurements of magnetization (M) vs. temperature were performed upon field cooling in a temperature range from 5–290 K and in an applied field (H) of 5000 Oe. The holder's diamagnetic contribution to the magnetization was subtracted when the raw data were converted to molar susceptibility ($\chi_m = M/H$). The susceptibility data plotted in Figures 2 and 3 were normalized per mol-Mn.

Computational Methodology: Electronic structure calculations were performed using the linear muffin-tin orbital (LMTO) method[41] implemented in the "LMTO 4.7" package.[42] All relativistic effects except for spin-orbit coupling were taken into account by a scalar relativistic approximation.[43] Electronic energies and magnetic moments were calculated via density-functional theory (DFT) based on the local-density approximation (LDA) for the exchange-correlation functional as parameterized by von Bath and Hedin[44] or based on the parameterization by Vosko, Wilk, and Nusari[45] augmented with gradient corrections[46] to follow the generalized-gradient approximation (GGA) with a total of 1000 k-points used in the irreducible Brillouin zone. Interstitial spheres were inserted to achieve space filling automatically.[47] The Fermi level was selected as the energy reference. To perform the spin-polarization calculations on $BaMn_2Sb_2$ and the imaginary $MgMn_2Sb_2$ compound (ordered structure), the symmetry of the system has to be lowered in order to treat the two Mn separately. In addition, in order to circumvent the problem with the statistically distributed Mn and Mg on the same crystallographic site in $Mg_{2.5}Mn_{0.5}Sb_2$, several $2 \times 2 \times 1$ super-cells were considered (Figure 7).

Supporting Information (see also the footnote on the first page of this article): Detailed description of the spin-polarized calculation of the hypothetical compound $MgMn_2Sb_2$, and a plot of the temperature dependence of the resistivity of $Mg_{2.50(3)}Mn_{0.50(3)}Sb_2$ (single crystal).

Acknowledgments

S. B. gratefully acknowledges funding from the University of Delaware and the Petroleum Research Fund (ACS-PRF). C. M. was financially supported by the 2007 NSF Summer Research Program in Solid State Chemistry. We are indebted to Arif Ozbay and Prof. Edmund R. Nowak from the Department of Physics and Astronomy for their help with the four-probe resistivity measurements.

[1] P. Villars, L. D. Calvert, *Pearson's Handbook of Crystallographic Data for Intermetallic Phases*, 2nd ed., American Society for Metals: Materials Park, OH, **1991**.
[2] C. Zheng, R. Hoffmann, *J. Solid State Chem.* **1988**, *72*, 58–71.
[3] D. Johrendt, C. Felser, O. Jepsen, O. K. Andersen, A. Mewis, J. Rouxel, *J. Solid State Chem.* **1997**, *130*, 254–265.
[4] C. Zheng, R. Hoffmann, R. Nesper, H.-G. von Schnering, *J. Am. Chem. Soc.* **1986**, *108*, 1876–1884.
[5] R. Hoffmann, C. Zheng, *J. Phys. Chem.* **1985**, *89*, 4175–4181.
[6] J. K. Burdett, G. J. Miller, *Chem. Mater.* **1990**, *2*, 12–26.
[7] F. Steglich, J. Aarts, C. D. Bredl, W. Lieke, D. Meschede, W. Franz, H. Schäfer, *Phys. Rev. Lett.* **1979**, *43*, 1892–1896.
[8] Z. Hossain, C. Geibel, F. Weickert, T. Radu, Y. Tokiwa, H. Jeevan, P. Gegenwart, F. Steglich, *Phys. Rev. B* **2005**, *72*, 094411.
[9] Z. Hossain, C. Geibel, T. Radu, Y. Tokiwa, F. Weickert, C. Krellner, H. Jeevan, P. Gegenwart, F. Steglich, *Phys. B* **2006**, *378–80*, 74–75.
[10] W. Jeitschko, R. Glaum, L. Boonk, *J. Solid State Chem.* **1987**, *69*, 93–100.
[11] T. Siegrist, H. W. Zandbergen, R. J. Cava, J. J. Krajewski, W. F. Peck, *Nature* **1994**, *367*, 254–256.
[12] T. K. Hatwar, R. M. Nayak, B. D. Padalia, M. N. Ghatikar, E. V. Sampathkumaran, L. C. Gupta, R. Vijayaraghavan, *Solid State Commun.* **1980**, *34*, 617–620.
[13] O. Tiedje, E. E. Krasovskii, W. Schattke, P. Stoll, C. Näther, W. Bensch, *Phys. Rev. B* **2003**, *67*, 134105.
[14] H. Winkelmann, M. M. Abd-Elmeguid, H. Micklitz, J. P. Sanchez, P. Vulliet, K. Alami-Yadri, D. Jaccard, *Phys. Rev. B* **1999**, *60*, 3324–3330.
[15] L. Moreschini, C. Dallera, J. J. Joyce, J. L. Sarrao, E. D. Bauer, V. Fritsch, S. Bobev, E. Carpene, S. Huotari, G. Vankó, G. Monaco, P. Lacovig, G. Panaccione, A. Fondacaro, G. Paolicelli, P. Torelli, M. Grioni, *Phys. Rev. B* **2007**, *75*, 035113.
[16] G. J. Snyder, E. S. Toberer, *Nat. Mater.* **2008**, *7*, 105–114.
[17] a) S. M. Kauzlarich, S. R. Brown, G. J. Snyder, *Dalton Trans.* **2007**, *21*, 2099–2100; b) F. Gascoin, S. Ottnsmann, D. Stark, S. M. Haile, G. J. Snyder, *Adv. Funct. Mater.* **2005**, *15*, 1860–1864.
[18] X.-J. Wang, M.-B. Tang, J.-T. Zhao, H.-H. Chen, X.-X. Yang, *Appl. Phys. Lett.* **2007**, *90*, 232107.
[19] a) C. L. Condron, S. M. Kauzlarich, F. Gascoin, G. J. Snyder, *J. Solid State Chem.* **2006**, *179*, 2252–2257; b) T. Kajikawa, N. Kimura, T. Yokoyama, in: *Proceedings of the 22nd International Conference on Thermoelectrics* **2003**, p. 305; c) F. Ahmadpour,

T. Kolodiazhnyi, Y. Mozharivskyj, *J. Solid State Chem.* **2007**, *180*, 2420–2428.
[20] S. L. Brock, J. E. Greedan, S. M. Kauzlarich, *J. Solid State Chem.* **1994**, *113*, 303–311.
[21] S. Bobev, J. Merz, A. Lima, V. Fritsch, J. D. Thompson, J. L. Sarrao, M. Gillessen, R. Dronskowski, *Inorg. Chem.* **2006**, *45*, 4047–4054.
[22] S.-Q. Xia, P. King, S. Bobev, *Acta Crystallogr., Sect. E* **2006**, *62*, I184–I186.
[23] *CRC Handbook of Chemistry and Physics*, 83rd ed., CRC Press LLC, New York, NY, **2002**.
[24] M. G. Kanatzidis, R. Pöttgen, W. Jeitschko, *Angew. Chem. Int. Ed.* **2005**, *44*, 6996–7023.
[25] E. Brechtel, G. Cordier, H. Schäfer, *Z. Naturforsch., Teil B* **1979**, *34*, 921–925.
[26] L. Pauling, *The Nature of the Chemical Bond*, 3rd ed., Cornell University Press, Ithaca, NY, **1960**.
[27] A direct comparison with the structure refined from single-crystal data is not significant as the two are done at different temperatures.
[28] C. Kittel, *Introduction to Solid-State Physics*, 7th ed., John Wiley & Sons, Inc., Hoboken, NJ, **1996**.
[29] D. Sánchez-Portal, R. M. Martin, S. M. Kauzlarich, W. E. Pickett, *Phys. Rev. B* **2002**, *65*, 144414.
[30] S.-Q. Xia, S. Bobev, *Inorg. Chem.* **2007**, *46*, 874–883.
[31] A. P. Holm, M. M. Olmstead, S. M. Kauzlarich, *Inorg. Chem.* **2003**, *42*, 1973–1981.
[32] H. Kim, C. L. Condron, A. P. Holm, S. M. Kauzlarich, *J. Am. Chem. Soc.* **2000**, *122*, 10720–10721.
[33] S.-M. Park, S.-J. Kim, M. G. Kanatzidis, *Inorg. Chem.* **2005**, *44*, 4979–4982.
[34] In cases like these, band calculations are known to overestimate the band-gap, and the pseudo band-gap that appears to open up at the Fermi level for $BaMn_2Sb_2$ may not indicate semiconducting properties.
[35] A. C. Payne, A. E. Sprauve, M. M. Olmstead, S. M. Kauzlarich, J.-Y. Chan, B. A. Reisner, J. W. Lynn, *J. Solid State Chem.* **2002**, *163*, 498–505.
[36] A. V. Morozkin, O. Isnard, P. Henry, S. Granovsky, R. Nirmala, P. Manfrinetti, *J. Alloys Compd.* **2006**, *420*, 34–36.
[37] W. Reimers, E. Hellner, W. Treutmann, P. J. Brown, *J. Phys. Chem. Solids* **1983**, *44*, 195–204.
[38] *Bruker SMART and SAINT*, Bruker AXS Inc., Madison, Wisconsin, USA, **2002**.
[39] G. M. Sheldrick, *SADABS*, University of Göttingen, Germany, **2003**.
[40] G. M. Sheldrick, *SHELXTL*, University of Göttingen, Germany, **2001**.
[41] a) O. K. Andersen, *Phys. Rev. B* **1975**, *12*, 3060–3083; b) O. K. Andersen, O. Jepsen, *Phys. Rev. Lett.* **1984**, *53*, 2571–2574; c) O. K. Andersen, O. Jepsen, D. Glötzel in *Highlights of Condensed Matter Theory* (Eds: F. Bassani, F. Fumi, M. P. Tosi), North Holland, **1985**, pp. 59–176; d) O. K. Andersen, Z. Pawlowska, O. Jepsen, *Phys. Rev. B* **1986**, *34*, 5253–5269; e) H. L. Skriver, *The LMTO Method*, Springer, Berlin, **1984**.
[42] O. Jepsen, O. K. Andersen, *The Stuttgart TB-LMTO Program, Version 4.7*.
[43] D. D. Koelling, B. N. Harmon, *J. Phys. C* **1977**, *10*, 3107–3114.
[44] U. von Barth, L. Hedin, *J. Phys. C* **1972**, *5*, 1629–1642.
[45] S. H. Vosko, L. Wilk, M. Nusair, *Can. J. Phys.* **1980**, *58*, 1200–1211.
[46] J. P. Perdew, J. A. Chevary, S. H. Vosko, K. A. Jackson, M. R. Pederson, C. Fiolhais, *Phys. Rev. B* **1992**, *46*, 6671–6687.
[47] O. Jepsen, O. K. Andersen, *Z. Phys. B* **1995**, *97*, 35–47.

Received: June 6, 2008
Published Online: August 15, 2008

